Published online 24 October 2006 *Nucleic Acids Research, 2006, Vol. 34, No. 20* ***5829–5838***
doi:10.1093/nar/gkl708

Structural basis of the *Methanothermobacter thermautotrophicus* MCM helicase activity

Alessandro Costa, Tillmann Pape[1], Marin van Heel[1], Peter Brick, Ardan Patwardhan[1] and Silvia Onesti*

Division of Cell and Molecular Biology and [1]Division of Molecular Biosciences, Faculty of Natural Sciences, Imperial College, London SW7 2AZ, UK

Received August 4, 2006; Revised September 12, 2006; Accepted September 13, 2006

ABSTRACT

The MCM complex from the archaeon *Methanothermobacter thermautotrophicus* is a model for the eukaryotic MCM2-7 helicase. We present electron-microscopy single-particle reconstructions of a DNA treated *M.thermautotrophicus* MCM sample and a ADP·AlF$_x$ treated sample, respectively assembling as double hexamers and double heptamers. The electron-density maps display an unexpected asymmetry between the two rings, suggesting that large conformational changes can occur within the complex. The structure of the MCM N-terminal domain, as well as the AAA+ and the C-terminal HTH domains of ZraR can be fitted into the reconstructions. Distinct configurations can be modelled for the AAA+ and the HTH domains, suggesting the nature of the conformational change within the complex. The pre-sensor 1 and the helix 2 insertions, important for the activity, can be located pointing towards the centre of the channel in the presence of DNA. We propose a mechanistic model for the helicase activity, based on a ligand-controlled rotation of the AAA+ subunits.

INTRODUCTION

In eukaryotic cells, six homologous proteins (MCM2-7) form a hetero-oligomer that is essential for DNA replication and is presumed to be the replicative helicase. The *Methanothermobacter thermautotrophicus* MCM (*Mth*MCM) homo-oligomeric complex is regarded as a simplified model for the study of the eukaryotic MCM2-7 complex (1). *Mth*MCM shares a high degree of sequence identity with the eukaryotic orthologues and displays DNA stimulated ATPase as well as helicase activities (2–4).

The *Mth*MCM protein can be divided into three domains: an N-terminal domain, a central AAA+ (ATPases Associated with various cellular Activities) domain and a C-terminal domain (Figure 1). Crystallographic studies have shown that the N-terminal domain forms a double-hexameric ring with a head-to-head configuration (5). The structure includes a β-hairpin, characterised by positively charged residues and shown to be involved in the interaction with DNA.

The central AAA+ domain can be divided into an α/β subdomain (the functional core of the enzyme) and an α subdomain mediating inter-subunit contacts. The α/β subdomain contains the Walker A, Walker B and arginine finger signature sequence motifs typical of AAA+ ATPases (6). No crystal structure is known for a MCM ATPase domain. Iyer *et al*. (7) carried out a systematic classification of AAA+ proteins and identified a superclade which includes the MCM proteins and is characterised by an insertion in the α/β subdomain occurring before the 'sensor 1' motif and forming a β-hairpin. This insertion has been called the pre-sensor 1 β-hairpin (PS1BH) and defines the superclade. Point mutation analysis of the *Sulfolobus solfataricus* MCM (*Sso*MCM) orthologue demonstrated that this insertion has a role in DNA binding and helicase activity (8). Within the PS1BH superclade, a number of AAA+ proteins contain an additional insertion in the α/β subdomain, disrupting the continuity of helix 2 (7). The helix 2 insertion (h2i) clade includes, among others, the MCM proteins, the BchI subunit of Mg-chelatase and the σ54-dependent bacterial transcriptional activators such as NtrC1 and ZraR (Supplementary Figure 1). According to the sequence alignments, the h2i in MCM corresponds to the GAFTGA motif insertion of the transcriptional activators and to a β–α–β insertion in the BchI subunit of Mg-chelatase (9). In MCM proteins, the h2i has been proposed to act as a ploughshare separating the two strands during the helicase reaction (1,10,11).

A detailed analysis of the α/β subdomains of proteins belonging to the h2i clade suggests that the MCM and bacterial transcriptional activators are closely related. In contrast, a structure-based sequence analysis of the α subdomains of proteins belonging to the h2i clade (12) suggests a closer similarity between MCM and BchI, as they both contain an insertion in the α subdomain (the pre-sensor 2 insertion) that adopts a helical conformation in BchI (9). This insertion confers a unique configuration to the region and potentially

*To whom correspondence should be addressed. Tel: +44 20 7594 7647; Fax: +44 20 75890191; Email: s.onesti@imperial.ac.uk

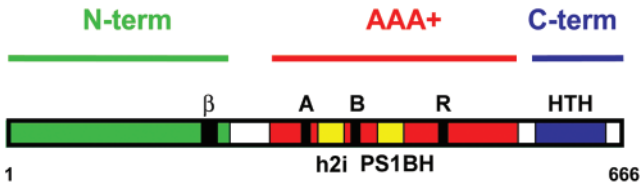

Figure 1. Domain structure of *Mth*MCM. The 242 amino acid N-terminal domain (green) contains a β-hairpin (β) capable of interacting with DNA. The central AAA+ domain (red) contains a Walker A, Walker B and arginine finger (R) motifs typical of AAA+ ATPases. In addition it contains a presensor 1 β-hairpin (PS1BH) insertion and a helix 2 insertion (h2i), highlighted in yellow. The C-terminal domain contains a predicted helix–turn–helix motif (HTH, blue).

influences the nature of inter-subunit contacts within the AAA+ ring assembly.

The C-terminal domain has yet to be characterised by structural studies. The last 100 amino acids of the *Mth*MCM protein include a predicted helix–turn–helix motif (HTH), a fold typical of DNA interacting domains (13). The HTH motif appears to be present in other archaeal MCM sequences but not in eukaryotic proteins.

A high degree of structural polymorphism has been reported for the MCM protein complexes from various organisms. The *Archeoglobus fulgidus* MCM and *Sso*MCM orthologues show hydrodynamic volumes compatible with the formation of single hexamers (14,15). Furthermore, *Sso*MCM binds a fork-shaped DNA substrate as a single ring (8). EM images of human MCM4/6/7 suggest a single ring configuration (16) and similar observations are reported for the *Schizosaccharomyces pombe* MCM complex (17). Gel filtration studies on the full-length *Mth*MCM protein suggest the formation of double rings (2–4) and EM single-particle studies on the same construct have shown that the protein can form either single or double rings, with either six or seven subunits per ring, where each ring is characterised by two tiers (18–20).

The observation of *Mth*MCM single rings by electron microscopy is likely to be due to the harsh treatment with uranyl acetate used for negative staining, but it indicates that the double ring is labile. Treatment with either nucleotides and/or dsDNA leads to the stabilisation of double ring structures, with a consistent shift to a double hexameric arrangement associated with DNA binding (21). This suggests that the double hexamer is the active form of the protein, with a possible role of the heptameric complex as a configuration ready to load onto DNA, as observed with related proteins (22,23).

The MCM protein is often compared to the functional homolog SV40 Large T antigen (LtAg) helicase (20). Both enzymes belong to the PS1BH superclade of AAA+ proteins and display common biochemical and structural features. They are characterised by the same 3′–5′ helicase activity and both show a double hexameric arrangement. They also both contain a positively charged central channel, believed to accommodate double stranded DNA (5,24), and lateral holes, possibly involved in the threading of single stranded DNA (18,24). The crystal structures of the LtAg in different nucleotide states show large conformational changes of the PS1BH insertion, which engages in an ATPase dependent spooling motion proposed to be responsible for the translocation along DNA (25,26). The fact that the h2i insertion found in MCM is missing in LtAg, has led to the suggestion that there may be fundamental differences in the helicase mechanism of the two enzymes (1).

Here we present electron microscopy single-particle reconstructions of *Mth*MCM treated with either the transition state analogue ADP·AlF_x or with a dsDNA fragment. In the presence of nucleotide the protein is arranged as a double heptamer, whereas in the presence of double stranded DNA it forms a double hexamer. We have fitted the atomic structures of the N-terminal domain of *Mth*MCM and the sequence-related AAA+ domain from the ZraR bacterial transcriptional activator (or the BchI subunit of Mg-chelatase) into the 3D maps. The results reveal the location of the C-terminal domain, the PS1BH and h2i insertions. Based on our fitting studies, we propose a ligand-controlled rotation of the AAA+ subunits, which provides new insights into the mechanism of action for the MCM helicase and suggests a model for preventing unnecessary ATPase hydrolysis when DNA is absent.

MATERIALS AND METHODS

Sample preparation, data acquisition and image processing

The detailed procedure for protein expression and purification, sample preparation and electron microscopy data acquisition have already been described in a preliminary single-particle analysis study (21). Image processing was performed with the IMAGIC-5 package (27). Single-particle reconstruction studies were carried out on particles from the DNA treated or the ADP·AlF_x treated samples. Micrographs were scanned using a Nikon Super Coolscan 8000 leading to a 1.3 Å/pixel size on the specimen scale. Pertinent (C6 or C7) symmetry was imposed on each model, according to the multivariate statistical analysis performed on top-view images (21,28) (Figure 2A). Only double-ring side and tilted views were used to generate the 3D reconstructions (Figure 2B) while ring-shaped top views were ignored. The resolution was determined using the Fourier shell correlation function at a threshold of 3σ multiplied by $\sqrt{6}$ or $\sqrt{7}$ according to the point group symmetry imposed. The resulting electron-density maps were filtered at the corresponding resolution using a Gaussian filter.

Fitting of X-ray structures

The docking of the N-terminal, central AAA+, and C-terminal rings was performed manually using O (29) and Pymol (30) and optimised using Situs (31). The handedness of the electron-density maps was determined by fitting the crystal structure of the *Mth*MCM N-terminal domain (5) (PDB accession code: 1LTL). The crystal structure of ZraR from *Salmonella typhimurium* (32) (PDB accession code: 1OJL) was used to generate a 6-fold and a 7-fold symmetric ring. This was fitted to the AAA+ ATPase domain of the double hexameric and double heptameric structures. The BchI subunit of Mg-chelatase from *Rhodobacter capsulatus* (9) (PDB accession code: 1G8P) was also used, after superimposing six copies of the monomer onto the ZraR hexamer. Visualisation of conformational changes within the AAA+ rings was performed by filtering the electron density derived

from the models to 20 Å resolution. Manipulation of the atomic coordinates and electron-density maps were performed using the CCP4 package (33).

RESULTS

Overall structure

Negative stain electron microscopy images of *Mth*MCM treated with either a dsDNA fragment or with ADP·AlF$_x$ were used for single-particle reconstruction studies. According to previous analyses, ring-shaped particles (top views) display 7-fold symmetry in the absence of DNA, but 6-fold symmetry when DNA is added (21) (Figure 2A). The pertinent symmetry was imposed in the reconstruction of the DNA treated protein (C6) and the ADP·AlF$_x$ treated protein (C7). For the purpose of reconstruction exploiting the presence of a symmetry axis (34), only double-ring side and tilted views were used while ring-shaped top views were ignored (Figure 2B). This allowed us to exclude easily corrupted information, such as single-ring and partially stained double-ring top views (21).

A 3D reconstruction was obtained for the dsDNA treated protein (double hexamer) based on a selection of 1060 particles (24 Å resolution, Figures 2B and 3A), and a reconstruction of the ADP·AlF$_x$ treated protein (double heptamer) was obtained based on 1940 particles (22 Å resolution, Figures 2B and 3B).

Both structures consist of a double-ring arrangement with a central channel and lateral holes. The height of both assemblies is ~200 Å while the double heptamer has a larger diameter consistent with the presence of an extra subunit in the heptameric ring. An asymmetry can be detected in both structures, with the lower ring consistently wider than the upper one (Figure 3C). The central channel is blocked in the upper ring of the double hexamer but is more open in the double heptamer.

As can be seen in a side-view slice through the middle of the DNA treated protein, electron density can be visualised inside the channel, in the centre of the upper but not the lower ring (Figure 3C). This density corresponds to a restriction of the DNA harbouring chamber, where elongated features of the protein point into the central channel. No electron density, nor any restriction, can be detected through the central channel of the double-heptameric structure. Finally, the holes visualised in the side walls of the MCM complex are large and continuous in the double-hexameric structure, but are instead divided into two apertures in the double-heptameric structure (Figure 3D).

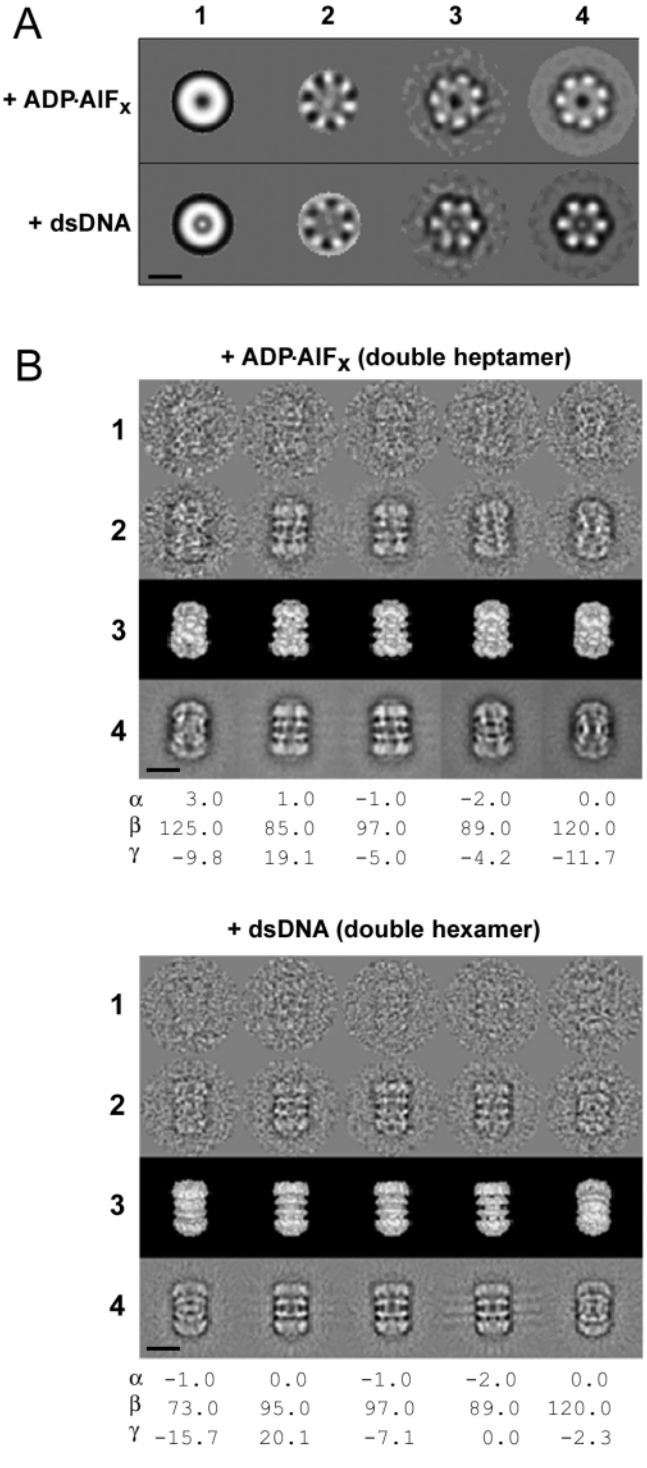

Figure 2. Single-particle analysis and 3D reconstruction. (**A**) Single-particle analysis performed on end-on views (21): (1) rotationally averaged total sum of end-on views; (2) most representative eigen images from end-on views, showing the symmetry component obtained performing MSA symmetry analysis; (3) characteristic end-on class averages obtained summing 100 images; (4) symmetry-imposed class averages. In the dsDNA treated protein, the particles present an intense peak of electron-density in the centre of the ring, which is lacking in the absence of DNA. This feature is particularly striking both in the rotationally averaged total sum and in the class averages. (**B**) Overview of the 3D reconstruction procedure of the double-hexameric and the double-heptameric structures (1) Examples of original images of *Mth*MCM stained with uranyl acetate. These images are members of the class averages shown in the row below (protein is white). (2) Class averages (characteristic views) obtained by multi-reference alignment and classification. (3) Surface representations of the 3D reconstruction viewed from directions identical to the Euler directions assigned to the corresponding class averages in 2. (4) Reprojections of the 3D structure in the Euler-angle directions found for the class averages in 2. Scale bar 100 Å. While carrying out the reconstruction, the pertinent symmetry was imposed according to the indication obtained from MSA symmetry analysis carried out on ring-shaped particles (end-on views, A). According to previous single-particle analysis studies (21), >90% of the particle population is consistent with the formation of double heptamers in the presence of ADP·AlF$_x$ and >80% of the particle population forms a double hexamer when treated with DNA.

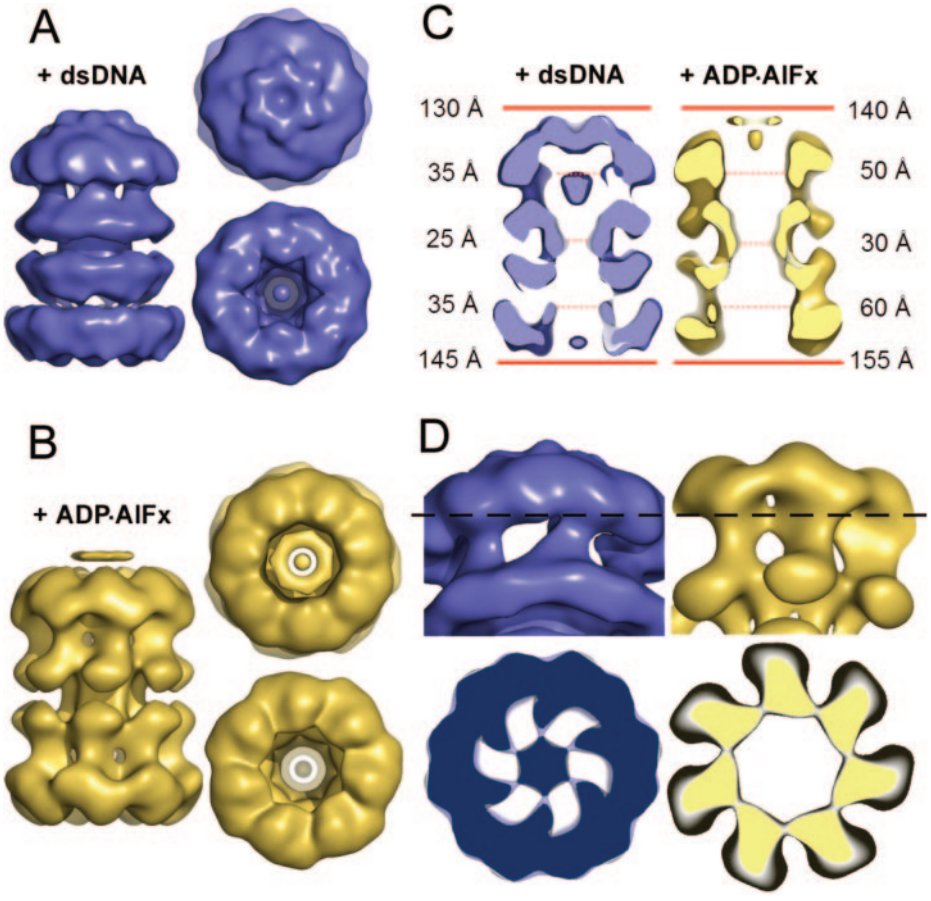

Figure 3. 3D reconstructions of *Mth*MCM complexes. Surface rendering of (**A**) the DNA treated MCM double hexamer (blue) and (**B**) the ADP·AlF_x treated double heptamer (yellow), showing a head-to-head double-ring configuration with lateral holes. The two rings display an asymmetry, which is more pronounced in the double hexamer. (**C**) Slice-through side views of the double hexamer (blue) and the double heptamer (yellow), showing the internal channel. The external diameter of the upper and lower rings (continuous red line) and the diameter of the channel (dotted red line) are shown on the sides for each of the reconstructions. The upper ring in the double hexamer shows the presence of electron density in the centre of the channel. The double heptamer has no large peak of electron density inside the channel, and wide chambers (50–60 Å) in the centre of the two rings. (**D**) A tilted view of the upper hexameric ring (blue) shows a single lateral hole per subunit; a section of the ring (at the level indicated by the dashed line) illustrates the presence of elongated features departing from the protein walls and pointing inside the central channel. A side-view of the upper heptameric ring (yellow) shows a lateral hole divided in two apertures by the presence of an isthmus of electron density, while a section emphasises the lack of any electron density pointing inside the central channel.

Model fitting of the N-terminal domain

The asymmetry, shown by both the DNA treated double hexamer and the nucleotide treated double heptamer, appears not to involve the domains at the interface between the two rings, but rather to be generated by the distal domains. In fact, the atomic coordinates of the symmetric *Mth*MCM N-terminal double hexamer (5) fit well into the electron density at the interface between the two rings (Figure 4A). Similar results were obtained by fitting a head-to-head dimer as a rigid body to the double-heptameric electron-density map and applying 7-fold symmetry to generate a heptameric N-terminal domain double ring (Figure 4B). Due to the resolution limit of the technique, no electron density can be visualised for the N-terminal β-hairpins.

Model fitting of the AAA+ domain suggests the location of the PS1BH and h2i elements

Since no atomic coordinates are available for the AAA+ domain of MCM proteins, the ZraR bacterial transcriptional activator from *S.typhimurium* was used (32). This protein belongs to the h2i clade and crystallised as a hexamer with a diameter appropriate for the size of the *Mth*MCM electron-density maps.

The orientation of the AAA+ module was chosen by reference to the LtAg protein (20,24). The assumption that the MCM and the LtAg helicase share the same orientation of the AAA+ tier is suggested by the fact that they both have 3′–5′ helicase activity and both display side channels at the interface between the N-terminal and AAA+ domains (18,20,24).

The crystal structure of ZraR was used to provide a 6-fold symmetric model for the AAA+ tier of the upper ring (Figure 5). The orientation resulting from docking the model into the upper ring of the double-hexamer map shows both the PS1BH and the h2i insertions pointing into the central channel (Figure 5B, C and E). The position of the PS1BH loops is similar to that observed in the LtAg helicase structure (24). The h2i elements extends towards the electron-density which protrudes from the walls of the

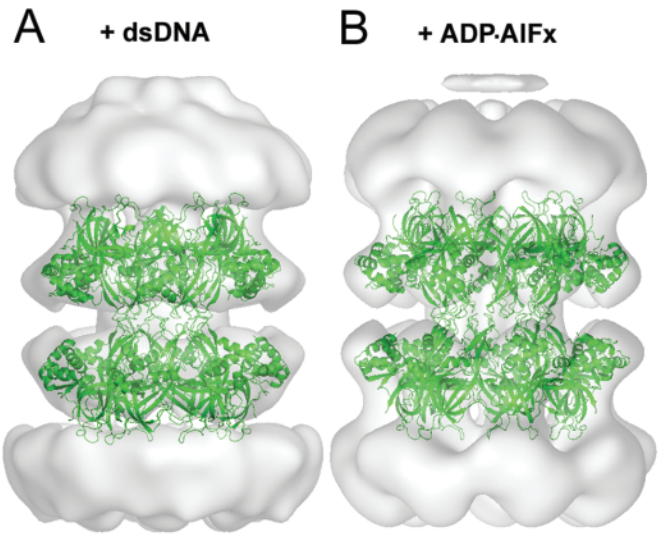

Figure 4. Fitting of the *Mth*MCM N-terminal domain. (**A**) Side-view of the atomic coordinates of the double hexameric N-terminal domain (5) (green) fitted into the electron-density map of the DNA treated sample. (**B**) A modelled heptameric N-terminal domain fitted into the electron density of the ADP·AlF_x treated sample. The good fit to the electron density suggests that the head-to-head symmetry shown by the crystal structure is also maintained in the single-particle reconstruction of the full-length protein.

chamber and meets on the symmetry axis; although the orientation of the PS1BH loops suggest they may also contribute to the protrusions, no electron-density is present for these elements, due to the fact that the low resolution achieved by electron microscopy does not allow for the definition of atomic details. We confirmed the assignment by generating the electron density of the ZraR model filtered to 20 Å resolution: an intense density peak in correspondence to the symmetry axis is produced, as observed in our reconstruction (Supplementary Figure 2).

Fitting the ZraR protein to the AAA+ tier of the lower ring in the double-hexamer map required a 10° rotation of the monomer about an axis parallel to the symmetry axis, causing a reorientation of the PS1BH and h2i elements away from the position they assume in the upper ring, so that rather than pointing inwards into the channel, they are now located against neighbouring subunits in the ring (Figure 5D and F). This domain rotation accounts for the difference in the ring diameters of the upper and lower rings in the double-hexamer. The type of movement observed is very similar to the conformational changes described for the LtAg helicase (25).

Fitting the ZraR protein to the AAA+ tier of both the upper and the lower rings in the double-heptameric electron-density map required an orientation of the monomer similar to that used for the lower ring of the double hexamer (Figure 5G–J). This caused the PS1BH and the h2i elements to turn away from the central channel to a position packing against the ring subunits. In this manner, PS1BH and h2i fit the additional electron density which disrupts the continuity of the lateral holes in the double heptamer. Only a small rearrangement of the AAA+ monomer was required to account for the differences between the upper and lower heptameric ring.

Crystallographic studies on various bacterial transcriptional activators describe a set of interactions between ring subunits, which are maintained despite differences in the oligomeric state of the protein (32,35,36). While modelling the inter-subunit rearrangements in *Mth*MCM we retained those interactions.

The atomic structure of BchI (9) was also considered as a candidate for the AAA+ domain, and modelling was carried out by superimposing six BchI monomers onto the ZraR hexamer. Because of the presence of the pre-sensor 2 insertion, the BchI hexamer displays a distinct shape in the peripheral α subdomain of the AAA+ module, resulting in a better fit to the outer belt of the upper hexameric MCM ring (Supplementary Figure 3). Nevertheless, because the sequence of the α/β subdomain of ZraR is closer to the MCM sequence and also possesses a HTH C-terminal domain, the BchI protein was not used in any further modelling.

Location of the C-terminal domain

After fitting the atomic structure of the hexameric AAA+ module of ZraR into the upper ring of the double-hexameric map, unassigned electron density remained on the cap of the ring and near the central channel (Figure 5A). An obvious candidate for this density is the 100 amino acid C-terminal domain, containing a predicted HTH domain of ~70 amino acids. We therefore choose to fit the crystal structure of the HTH motif from the C-terminus of ZraR into the residual electron density (Figure 6A).

We also placed the crystal structure of the ZraR HTH motif into the unassigned density of the lower hexameric ring. An optimum fit was obtained with the HTH C-terminal domain displaced by 10 Å towards the AAA+ module compared with the position in the upper ring (Figure 6A).

The same approach was followed for the fitting of the double-heptameric electron-density map, using the AAA+ and C-terminal domains as a rigid body, locked in the configuration used for the hexameric lower ring (Figure 6C). Surface representations of the modelled double-ring structures emphasises the different positions of the C-terminal domains in the two complexes (Figure 6B and D).

Despite the fact that the double heptamer lacks the striking cap structure seen in the upper ring of the double-hexamer, the reconstruction of the upper ring includes some residual electron density surrounding the symmetry axis (Figure 3B and C). Although we did not attempt to fit any atomic model into this density, it is also possible that the feature may represent a partially ordered C-terminal domain.

DISCUSSION

New insights into the MCM helicase activity

Despite the lack of high resolution data for the central AAA+ and the C-terminal domains of the archaeal MCM helicases, a wealth of sequence analysis and biochemical information have become available which shed light on the molecular mechanism of the MCM helicase.

Site directed mutagenesis studies of the PS1BH insertion in the AAA+ domain of the *Sso*MCM orthologue demonstrated

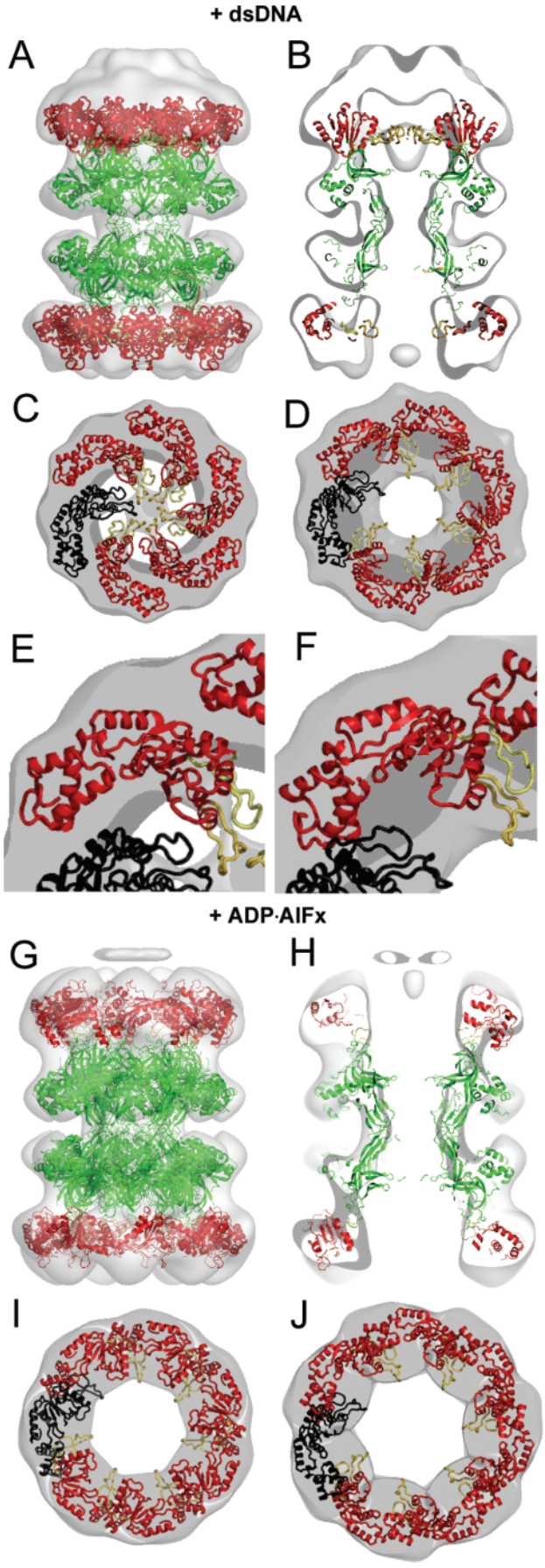

its crucial role for DNA binding and helicase activity (8). Fluorescence studies suggest a DNA-triggered movement of the h2i in *Mth*MCM, which has been shown to be necessary for helicase activity and was proposed to act as a ploughshare (11). In the SV40 LtAg helicase the PS1BH insertion engages in a nucleotide-dependent spooling motion which has been proposed to be coupled to dsDNA translocation and unwinding (25). Another critical residue in LtAg is phenylalanine 459 in helix 2 (24) (Supplementary Figure 1), which moves in concert with PS1BH (25) and is believed to act as a ploughshare that separates the two strands of DNA (26). The position of this phenylalanine coincides with the helix 2 insertion in MCM proteins. In the ZraR protein and in all the transcriptional activators of the same family, the helix 2 insertion corresponds to the GAFTGA loop, whose conformational change upon nucleotide binding and hydrolysis is also believed to be critical for the activity (37,38).

In the upper ring of the *Mth*MCM sample treated with DNA, we can see some electron density protruding from the internal walls of the protein ring towards the centre of the DNA channel. Modelling ZraR or BchI into the electron density allowed us to assign this electron density to the h2i elements, possibly with a contribution of the PS1BH (Figure 5). This electron density is not present in the lower ring of the hexameric complex, nor in the heptameric complex, suggesting that large conformational changes takes place moving the loops away from the centre of the channel. Based on those changes, we can model a movement (Figure 7) which is reminiscent of the nucleotide-state dependent iris-type motion of the LtAg helicase (25). This interpretation is consistent with the proposed biochemical role of the PS1BH and the h2i, respectively believed to be involved in the active translocation along DNA and in the separation of the two strands. The necessity of using a whole 'arm' as a ploughshare (the h2i in MCM) instead of a single residue (F459 in LtAg) is consistent with the larger diameter of the central channel of MCM compared to the LtAg hexameric ring.

Docking of the atomic structure of the BchI subunit of Mg-chelatase onto the upper hexameric ring results in a better fit to the electron density of the outer belt of the AAA+ module (Supplementary Figure 3), compared to the results obtained for ZraR (Figure 5). This confirms the closer similarity in the architecture of the peripheral α subdomain between the BchI and MCM protein, as suggested by the structure-guided sequence alignment studies (12).

Figure 5. Fitting of the AAA+ ATPase domain of the ZraR transcriptional activator. The atomic coordinates of ZraR model derived from the crystal structure (32) were fitted to the AAA+ modules of MCM. The AAA+ domain of ZraR is shown in red, whereas the N-terminal domain of *Mth*MCM is shown in green. One AAA+ subunit is colored in black. (**A**) Side-view of the double hexamer. (**B**) Side-view section of the double hexamer. (**C**) Section through the top ring of the double hexamer. (**D**) Section through the bottom ring of the double hexamer. (**E**) Close-up of the section of the top ring shown in (C). The h2i and PS1BH (shown in yellow) are pointing into the central channel and account for the electron density. (**F**) Close-up of the section of the bottom ring shown in D. The h2i and PS1BH (shown in yellow) pack against the ring subunits. (**G**) Side-view of the double heptamer. (**H**) Side-view section of the double hexamer. (**I**) Section through the top ring of the double heptamer. (**J**) Section through the bottom ring of the double heptamer. In the model of the double heptamer, the h2i and PS1BH pack between subunits in both the upper and lower rings.

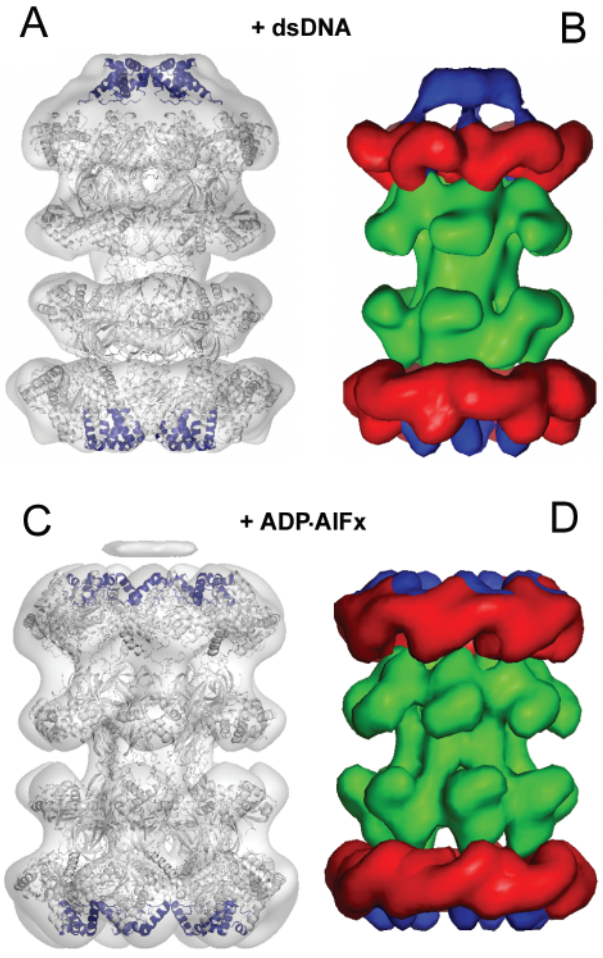

Figure 6. Proposed location of the C-terminal domain. (**A**) The crystal structure of the HTH motif from the C-terminus of ZraR (blue) fitted into the 3D reconstruction of the double hexamer. Different relative positions of the C-terminal domain and AAA+ domains have been used to fit the upper and lower rings. (**B**) Surface representation obtained by filtering to 20 Å resolution the electron density calculated from the modelled atomic structures. The N-terminal domain is shown in green, the AAA+ domain in red and C-terminal domain in blue. (**C**) The crystal structure of the HTH motif from the C-terminus of ZraR (blue) fitted into the 3D reconstruction of the double heptamer. The AAA+ and C-terminal domains are in the same relative orientation as in the lower hexameric ring. (**D**) Surface representation of the heptameric model calculated and coloured as in (B).

The C-terminal domain

A deletion mutant of the *Mth*MCM protein lacking the C-terminal domain showed an enhanced DNA-stimulated ATPase activity compared to the wild-type protein, but lower helicase activity, together with a smaller DNA-induced conformational change observed by steady state fluorescence (11). FRET experiments on the *Sso*MCM also suggested a DNA-induced conformational change involving the C-terminal domain (8). These observations indicate a possible role for the C-terminal domain in coupling the ATP hydrolysis and DNA spooling motion necessary for the helicase activity. We can visualise conformational changes in the MCM complex and our model directly involves a major rearrangement of the C-terminal domain (Figures 6 and 7).

Evidence for the mobility of a HTH containing C-terminal domain is also found in various bacterial transcriptional activators. The X-ray structure of ZraR revealed two different conformations of the HTH domain (32) and EM single-particle reconstruction studies of the homologous NtrC1 protein, report a nucleotide-dependent stabilisation of the DNA-binding HTH C-terminal domain at the top of the AAA+ ring and in close proximity to the central channel (37). A similar position was proposed for the HTH C-terminal domain of RuvB, which has been suggested to play an important role in translocating dsDNA out of the central channel (39).

In a previous analysis of the EM reconstruction of a hexameric *Mth*MCM complex, after fitting the AAA+ domain derived from RuvB, it was suggested that the C-terminal domain was located between the N-terminal and AAA+ domains (18). The latest bioinformatics and biochemical data on the AAA+ and MCM proteins, together with the presence of the electron density corresponding to the PS1BH and h2i insertions in our DNA treated sample, have allowed us to use a better model for the AAA+ domain and to obtain a more accurate fit using a revised position for the C-terminal domain. This position is still compatible with the FRET measurements obtained for the SsoMCM protein, which showed that the distance between the C-terminal and the N-terminal domains is ~75 Å (8).

We modelled various locations for the C-terminal domain in our reconstructions (Figure 6) but we feel that these should be treated with different degrees of confidence. We are confident about the positioning of the C-terminal domain in the upper hexamer of the DNA treated sample. The domain stands out with respect to the body of the core AAA+ domain, making the modelling into a low resolution map easier; moreover, a similar position has been proposed for the HTH domain of other two AAA+ proteins, namely NtrC1 (37) and RuvB (39). We are less sure about the relocation of the C-terminal domain away from the symmetry axis in the other instances, since the density is not clearly separated from that of the AAA+ domain. An alternative explanation would be a conformational change involving an order–disorder transition, as proposed for the transcriptional activator NtrC1 (37). Indeed, some residual density close to the symmetry axis can be seen both in the bottom ring of the double hexamer and the top ring of the double heptamer (Figure 3C) and could be interpreted as a partially disordered C-terminal domain.

DNA binding causes inter-subunit rearrangements which could trigger ATP hydrolysis

The structural basis of polynucleotide-stimulated ATPase activity has been characterised at a molecular level for the Rho transcription termination factor, where RNA binding is believed to cause the transition from a lock-wash to a closed-ring structure and the concomitant reconfiguration of the ATPase active site (40). Similarly, we see a transition from a heptameric to a hexameric ring upon DNA binding, which could affect the subunit interface, disrupting the ATPase active site when DNA is absent or reconstituting it when DNA is added. Our model fitting suggests a crucial role for the h2i and PS1BH insertions in this conformational change (Figure 7). In agreement with this model, the h2i deletion mutant of *Mth*MCM shows a higher DNA stimulated

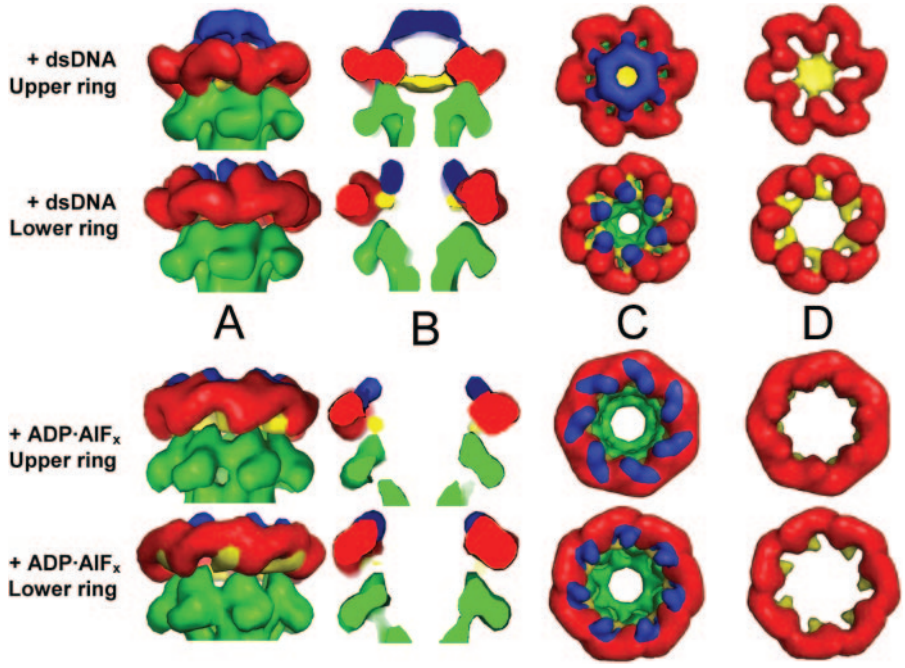

Figure 7. Surface representation of the conformational changes occurring within the *Mth*MCM rings. The N-terminal domain is shown in green, the AAA+ domain in red, the PS1BH and h2i insertions in yellow and the C-terminal domain in blue. To simplify the comparison with the upper rings, the lower rings have been inverted. The structures are viewed from (**A**) the side, (**B**) a slice through the side, (**C**) the top and (**D**) the top after the N- and C-terminal domains have been removed. The conformational changes within the upper and lower rings of the double hexamer are reminiscent of the nucleotide-controlled iris-type motion described for the LtAg helicase (25). Such a movement involves both the AAA+ and the C-terminal domain. Due to a rotation of the AAA+ domain, the PS1BH and h2i insertions move from pointing inside the channel to an inter-subunit position. Concertedly, the C-terminal domain rearranges from forming a distinct cap on top of the AAA+ tier to a less extended configuration.

ATPase activity (11) and mutants affecting PS1BH show levels of ATPase activity in the absence of DNA as high as that of the wild-type in the presence of DNA (8).

Although a double-hexameric reconstruction for *Mth*MCM has been already reported (20), the AAA+ is poorly defined, there is no electron density for the C-terminal domain and there is no indication of asymmetry between the two rings. The asymmetry we observe within the double-ring structure, particularly evident in the case of the MCM:DNA complex, suggests some level of negative cooperativity within the complex, and possibly indicates that only one of the two rings is binding DNA. Since the interactions between the two rings are mediated by the N-terminal domain, any asymmetry involving the AAA+ domain requires some cross-talk between the N-terminal domains and the rest of the protein (21), as well as some degree of asymmetry within the N-terminal domains. However these subtle changes within the N-terminal domain are probably too small to be detected by electron microscopy at 22 Å resolution.

Noticeably, DNA-triggered conformational changes are presented here, although no DNA could actually be visualised throughout the central channel. The lack of any electron-density accounting for the presence of DNA has been reported in a number of DNA-treated protein single-particle reconstruction studies (41,42) and is likely to be due to the mobility of the DNA inside the central channel and to the limits imposed by the negative staining technique itself. However, a body of circumstantial evidence strongly suggests that a high percentage of the sample is in complex with DNA. Treatment with dsDNA causes a macroscopic change in stoichiometry, from an unliganded *Mth*MCM which is mostly heptameric to a sample that is mostly a double hexamer (Figure 2A). This is also true when the sample is treated with DNA in the presence of other ligands, such as ADP·AlF$_x$ and AMP-PNP (21). Moreover, treatment with dsDNA is associated with the presence of a peak of electron density blocking the channel of the upper hexamer, density that we interpret as the ordering or the relocation of the PS1BH and h2i elements. Again, identical results are obtained for samples treated with dsDNA and either ADP·AlF$_x$ or AMP-PNP (A. Costa and A. Patwardhan, unpublished data).

Although the observation of different arrangements for the AAA+ and C-terminal domains gives an indication of the type of conformational changes that can occur in the MCM complex during the catalytic cycle, we still do not have a full explanation for how ATP binding and hydrolysis drive the translocation and melting of DNA. In particular, we cannot provide an obvious correlation between the nucleotide-state of the complex and its configuration. A more detailed analysis of all the possible states of the molecules is needed, leading to 3D reconstructions that provide snapshots of the complex along the reaction pathway. Crystallographic data on the AAA+ and C-terminal domains will also be needed to complete the picture and supply an atomic model for the missing building blocks in the MCM complex.

However, our single-particle reconstruction and model fitting studies provide a key for interpreting the latest biochemical characterisation of the MCM helicase, as they represent the first structural evidence to locate the PS1BH and h2i insertions and to model their conformational changes,

which are believed to be essential for the modulation of the helicase activity. Moreover we see clear electron density for the C-terminal HTH domain and observe that this region undergoes a structural transition dependent on the functional state of the molecule.

SUPPLEMENTARY DATA

Supplementary Data are available at NAR Online.

ACKNOWLEDGEMENTS

We are grateful to Jean Gautier for providing the *Mth*MCM expression construct and to Mathieu Rappas and Jörg Schumacher for fruitful discussions. This work was supported by a EU grant to MvH (EC contract LSHG-CT-2004-502828) and by an Imperial College Faculty Research Initiative grant to S.O. and A.P. Funding to pay the Open Access publication charges for this article was provided by internal college funding.

Conflict of interest statement. None declared.

REFERENCES

1. Chong,J.P. (2005) Learning to unwind. *Nature Struct. Mol. Biol*., **12**, 734–736.
2. Chong,J.P., Hayashi,M.K., Simon,M.N., Xu,R.M. and Stillman,B. (2000) A double-hexamer archaeal minichromosome maintenance protein is an ATP-dependent DNA helicase. *Proc. Natl Acad. Sci. USA*, **97**, 1530–1535.
3. Shechter,D.F., Ying,C.Y. and Gautier,J. (2000) The intrinsic DNA helicase activity of Methanobacterium thermoautotrophicum delta H minichromosome maintenance protein. *J. Biol. Chem*., **275**, 15049–15059.
4. Kelman,Z., Lee,J.K. and Hurwitz,J. (1999) The single minichromosome maintenance protein of Methanobacterium thermoautotrophicum DeltaH contains DNA helicase activity. *Proc. Natl Acad. Sci. USA*, **96**, 14783–14788.
5. Fletcher,R.J., Bishop,B.E., Leon,R.P., Sclafani,R.A., Ogata,C.M. and Chen,X.S. (2003) The structure and function of MCM from archaeal M. thermoautotrophicum. *Nature Struct. Biol*., **10**, 160–167.
6. Koonin,E.V. (1993) A common set of conserved motifs in a vast variety of putative nucleic acid-dependent ATPases including MCM proteins involved in the initiation of eukaryotic DNA replication. *Nucleic Acids Res*., **21**, 2541–2547.
7. Iyer,L.M., Leipe,D.D., Koonin,E.V. and Aravind,L. (2004) Evolutionary history and higher order classification of AAA+ ATPases. *J. Struct. Biol*., **146**, 11–31.
8. McGeoch,A.T., Trakselis,M.A., Laskey,R.A. and Bell,S.D. (2005) Organization of the archaeal MCM complex on DNA and implications for the helicase mechanism. *Nature Struct. Mol. Biol*., **12**, 756–762.
9. Fodje,M.N., Hansson,A., Hansson,M., Olsen,J.G., Gough,S., Willows,R.D. and Al-Karadaghi,S. (2001) Interplay between an AAA module and an integrin I domain may regulate the function of magnesium chelatase. *J. Mol. Biol*., **311**, 111–122.
10. Takahashi,T.S., Wigley,D.B. and Walter,J.C. (2005) Pumps, paradoxes and ploughshares: mechanism of the MCM2-7 DNA helicase. *Trends Biochem. Sci*., **30**, 437–444.
11. Jenkinson,E.R. and Chong,J.P. (2006) Minichromosome maintenance helicase activity is controlled by N- and C-terminal motifs and requires the ATPase domain helix-2 insert. *Proc. Natl Acad. Sci. USA*, **103**, 7613–7618.
12. Erzberger,J.P. and Berger,J.M. (2006) Evolutionary relationships and structural mechanisms of AAA+ proteins. *Annu. Rev. Biophys. Biomol. Struct*., **35**, 93–114.
13. Aravind,L. and Koonin,E.V. (1999) DNA-binding proteins and evolution of transcription regulation in the archaea. *Nucleic Acids Res*., **27**, 4658–4670.
14. Carpentieri,F., De Felice,M., De Falco,M., Rossi,M. and Pisani,F.M. (2002) Physical and functional interaction between the mini-chromosome maintenance-like DNA helicase and the single-stranded DNA binding protein from the crenarchaeon *Sulfolobus solfataricus*. *J. Biol. Chem*., **277**, 12118–12127.
15. Grainge,I., Scaife,S. and Wigley,D.B. (2003) Biochemical analysis of components of the pre-replication complex of *Archaeoglobus fulgidus*. *Nucleic Acids Res*., **31**, 4888–4898.
16. Sato,M., Gotow,T., You,Z., Komamura-Kohno,Y., Uchiyama,Y., Yabuta,N., Nojima,H. and Ishimi,Y. (2000) Electron microscopic observation and single-stranded DNA binding activity of the Mcm4,6,7 complex. *J. Mol. Biol*., **300**, 421–431.
17. Adachi,Y., Usukura,J. and Yanagida,M. (1997) A globular complex formation by Nda1 and the other five members of the MCM protein family in fission yeast. *Genes Cells*, **2**, 467–479.
18. Pape,T., Meka,H., Chen,S., Vicentini,G., van Heel,M. and Onesti,S. (2003) Hexameric ring structure of the full-length archaeal MCM protein complex. *EMBO Rep*., **4**, 1079–1083.
19. Yu,X., VanLoock,M.S., Poplawski,A., Kelman,Z., Xiang,T., Tye,B.K. and Egelman,E.H. (2002) The Methanobacterium thermoautotrophicum MCM protein can form heptameric rings. *EMBO Rep*., **3**, 792–797.
20. Gomez-Llorente,Y., Fletcher,R.J., Chen,X.S., Carazo,J.M. and San Martin,C. (2005) Polymorphism and double hexamer structure in the archaeal minichromosome maintenance (MCM) helicase from Methanobacterium thermoautotrophicum. *J. Biol. Chem*., **280**, 40909–40915.
21. Costa,A., Pape,T., van Heel,M., Brick,P., Patwardhan,A. and Onesti,S. (2006) Structural studies of the archaeal MCM complex in different functional states. *J. Struct. Biol.,* Online publication. doi:10.1016/j.jsb.2006.04.001.
22. Miyata,T., Yamada,K., Iwasaki,H., Shinagawa,H., Morikawa,K. and Mayanagi,K. (2000) Two different oligomeric states of the RuvB branch migration motor protein as revealed by electron microscopy. *J. Struct. Biol*., **131**, 83–89.
23. Crampton,D.J., Ohi,M., Qimron,U., Walz,T. and Richardson,C.C. (2006) Oligomeric states of Bacteriophage T7 Gene 4 primase/helicase. *J. Mol. Biol*., **360**, 667–677.
24. Li,D., Zhao,R., Lilyestrom,W., Gai,D., Zhang,R., DeCaprio,J.A., Fanning,E., Jochimiak,A., Szakonyi,G. and Chen,X.S. (2003) Structure of the replicative helicase of the oncoprotein SV40 large tumour antigen. *Nature*, **423**, 512–518.
25. Gai,D., Zhao,R., Li,D., Finkielstein,C.V. and Chen,X.S. (2004) Mechanisms of conformational change for a replicative hexameric helicase of SV40 large tumor antigen. *Cell*, **119**, 47–60.
26. Shen,J., Gai,D., Patrick,A., Greenleaf,W.B. and Chen,X.S. (2005) The roles of the residues on the channel beta-hairpin and loop structures of simian virus 40 hexameric helicase. *Proc. Natl Acad. Sci. USA*, **102**, 11248–11253.
27. van Heel,M., Harauz,G., Orlova,E.V., Schmidt,R. and Schatz,M. (1996) A new generation of the IMAGIC image processing system. *J. Struct. Biol*., **116**, 17–24.
28. Dube,P., Tavares,P., Lurz,R. and van Heel,M. (1993) The portal protein of bacteriophage SPP1: a DNA pump with 13-fold symmetry. *EMBO J*., **12**, 1303–1309.
29. Jones,T.A., Zou,J.Y., Cowan,S.W. and Kjeldgaard,M. (1991) Improved methods for building protein models in electron density maps and the location of errors in these models. *Acta Crystallogr. A*, **47**, 110–119.
30. DeLano,W.L. (2002) *The Pymol Molecular Graphics system, DeLano Scientific*. San Carlos, CA, USA.
31. Wriggers,W., Milligan,R.A. and McCammon,J.A. (1999) Situs: a package for docking crystal structures into low-resolution maps from electron microscopy. *J. Struct. Biol*., **125**, 185–195.
32. Sallai,L. and Tucker,P.A. (2005) Crystal structure of the central and C-terminal domain of the sigma(54)-activator ZraR. *J. Struct. Biol*., **151**, 160–170.
33. Collaborative Computational Project, Number 4 (1994) The CCP4 suite: programs for protein crystallography. *Acta Crystallogr. D Biol. Crystallogr*., **50**, 760–763.
34. Boisset,N., Penczek,P.A., Taveay,J.C., You,V., de Haas,F. and Lamy,J. (1998) Overabundant single-particle electron microscope views induce a three-dimensional reconstruction artifact. *Ultramicroscopy*, **74**, 201–207.
35. Rappas,M., Schumacher,J., Beuron,F., Niwa,H., Bordes,P., Wigneshweraraj,S., Keetch,C.A., Robinson,C.V., Buck,M. and Zhang,X. (2005) Structural insights into the activity of enhancer-binding proteins. *Science*, **307**, 1972–1975.
36. Lee,S.Y., De La Torre,A., Yan,D., Kustu,S., Nixon,B.T. and Wemmer,D.E. (2003) Regulation of the transcriptional activator NtrC1:

structural studies of the regulatory and AAA+ ATPase domains. *Genes Dev*., **17**, 2552–2563.
37. De Carlo,S., Chen,B., Hoover,T.R., Kondrashkina,E., Nogales,E. and Nixon,B.T. (2006) The structural basis for regulated assembly and function of the transcriptional activator NtrC. *Genes Dev*., **20**, 1485–1495.
38. Schumacher,J., Joly,N., Rappas,M., Zhang,X. and Buck,M. (2006) Structures and organisation of AAA+ enhancer binding proteins in transcriptional activation. *J. Struct. Biol.,* Online publication. doi:10.1016/j.jsb.2006.01.006.
39. Yamada,K., Miyata,T., Tsuchiya,D., Oyama,T., Fujiwara,Y., Ohnishi,T., Iwasaki,H., Shinagawa,H., Ariyoshi,M., Mayanagi,K. *et al.* (2002) Crystal structure of the RuvA-RuvB complex: a structural basis for the Holliday junction migrating motor machinery. *Mol. Cell*, **10**, 671–681.
40. Skordalakes,E. and Berger,J.M. (2003) Structure of the Rho transcription terminator: mechanism of mRNA recognition and helicase loading. *Cell*, **114**, 135–146.
41. Valle,M., Chen,X.S., Donate,L.E., Fanning,E. and Carazo,J.M. (2006) Structural basis for the cooperative assembly of large T antigen on the origin of replication. *J. Mol. Biol*., **357**, 1295–1305.
42. Chen,Y.J., Yu,X. and Egelman,E.H. (2002) The hexameric ring structure of the Escherichia coli RuvB branch migration protein. *J. Mol. Biol*., **319**, 587–591.